Soft Matter

COMMUNICATION

View Article Online
View Journal | View Issue



Cite this: *Soft Matter*, 2017, 13, 3841

Received 20th January 2017,
Accepted 4th May 2017

DOI: 10.1039/c7sm00147a

rsc.li/soft-matter-journal



# Extensive characterization of magnetic microrods observed using optical microscopy†

Fabien Gerbal, *[ab] Yuan Wang,[a] Olivier Sandre,[c] Fabien Montel[a] and Jean-Claude Bacri[a]

**The usage of micro or nanorods is steadily increasing in various applications from fundamental research to industry. Therefore their geometrical, mechanical and eventually magnetic properties need to be well determined. Here, using an optical microscope equipped with magnetic tweezers, we report an experimental procedure to obtain all those information on a single magnetic rod. In particular, we measure magnetic susceptibility $\chi$ by analyzing the deformation of a rod subjected to a uniform magnetic field. To do so, we refine a theoretical model which takes into account the variation of $\chi$ with the internal field. We prove experimentally that this model yields consistent measurements, at any value of the field strength and the incidence angle. From the combination of the different measurements, we also deduce the number of iron oxide nanoparticles which are embedded within the polymer matrix of the superparamagnetic rods under study.**

A very broad research activity concerns micro and nanoscale magnetic rods which show fundamental interest in many applications such as surface coating reagents, actuators, bio-medical probes and so on.[4] Depending on their size, various strategies have been developed to synthesize them: near-micron radius or larger wires are made for instance from rapid quenching,[20] whereas the probably most common strategy for preparing rods around tens of nanometers diameter consists in filling the pores of an etched template by electrochemical deposition of one or several metals.[6] Other groups realized nanorods by metallizing bacteria,[14] by chaining particles together,[17] or by embodying nanoparticles into an elastomer gel such as PDMS through lithographic techniques.[18] Many applications for which these rods are designed require a well-characterized calibration of their properties, often at the level of the individual object rather than for a broad distribution.

We report the measurements of the length $L$, radius $r$, flexural rigidity $C$, and magnetic susceptibility $\chi$ performed on single individual rods by using a conventional optical microscope equipped with magnetic tweezers (ESI,† note 1 shows the complete scheme of all measurements). Whereas the measurements presented in this paper could be applied to many types of magnetic rods, we studied $r \sim$ 200–400 nm, $L \sim$ 10–80 micron-long superparamagnetic rods made of $\sim$13 nm diameter iron oxide nanoparticles embedded into a polymer matrix.[3,7,11,12,19] We initially assessed each measurement independently: the super-resolutive optical model used to derive $r$ was compared to Atomic Force Microscopy (AFM) scans performed on the same rods; the measured value of $C$ was derived from the analysis of the thermal fluctuations;[11] $\chi$ was obtained from the measurement of the tip deflection of a magnetically-bent rod. To do so, we used a theoretical model (which takes into account the variation of $\chi(H)$ with the field strength $H$[12]) to describe the magnetoelastic deformation of rods. We present an improved version of this model which applies well to rods of relatively low magnetic susceptibility such as the ones studied here. By comparison of the resulting $\chi$ value with the susceptibility $\chi^p$ of the particles which compose the rods (measured independently using vibrating sample magnetometry (VSM)), we deduced the volume fraction $\phi$ of the magnetic nanoparticles. We also report experiments which yield constant values for $\phi$, independently of the intensity and the incidence angle of the field, thereby demonstrating the robustness of the model. Finally, the full analysis performed on 10 different rods showed consistent and relatively low dispersion of the values found for $\phi \sim$ 10–30% considering the broad disparity of $\chi \sim$ 2.0–7.4 (at $\mu_0 H$ = 4 mT) and $C \sim 10^{-18}$–$10^{-20}$ Jm.

$\gamma$-$Fe_2O_3$ (maghemite) iron oxide nano-particles which compose the rods were synthesized by the aqueous coprecipitation route also called the Massart procedure, followed by a size sorting procedure.[1] Their nanometric size yields their superparamagnetic

[a] *Laboratoire Matière et Systèmes Complexes (MSC) UMR 7057 (CNRS) and Université Denis Diderot – Sorbonne Paris Cité, 10 rue Alice Domon et Léonie Duquet, 75013 Paris, France. E-mail: fabien.gerbal@upmc.fr; Fax: +33 (0)1 57 27 62 11; Tel: +33 (0)1 57 27 62 88*

[b] *Université Pierre et Marie Curie – Paris 6, Sorbonne Universités, 4 place Jussieu, 75252 Paris Cedex 05, France*

[c] *CNRS and Université de Bordeaux, Laboratoire de Chimie des Polymères Organiques (LCPO), UMR 5629, F-33600 Pessac, France*

† Electronic supplementary information (ESI) available. See DOI: 10.1039/c7sm00147a

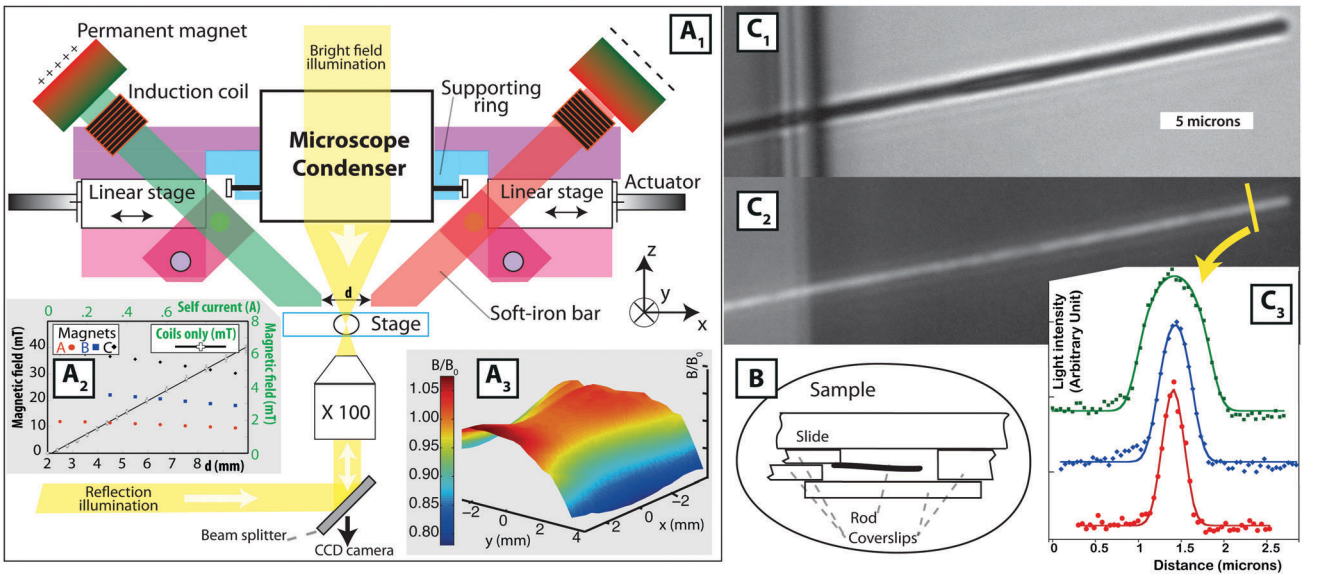


Fig. 1 Experimental setup and rod images. ($A_1$) Microscope setup equipped with magnetic tweezers. The sample may be observed by standard bright field or by reflection microscopy by use of a beam splitter. Set on a ring attached to the condenser of the inverted microscope, the magnetic device is free to rotate in the ($x$, $y$) plane perpendicular to the microscope light path. It consists of two 7 cm diameter soft iron bars, planed at one end so they can be brought in the vicinity of the sample. They are mounted on actuated stages in order to vary the distance $d$ between their tips (precision $\sim$10 μm). The magnetic field is induced by permanent magnets or by induction coils at the remote end of these bars. The axial symmetry of the system ensures that the field in the midperpendicular plane is horizontal. The magnets were used to demagnetize the bar before each experiments, and fine-tuned magnetic field could be generated by use of the coils (powered by a computer-controlled DC generator) without producing mechanical disturbances. ($A_2$) Calibration of the $x$-component of the field at the expected position of the rod, for (i) a set of three magnets as a function of $d$ (axis in black) and (ii) as a function of the current in the coils (axis in green), for $d$ = 2.5 mm and without magnet. The $\sim$2% error bars are mostly due to the uncertainty on the sample position along $z$ ($\sim$10 μm) and the weak vertical field gradient ($\partial B_x/\partial z \sim 0.6$ T m$^{-1}$). ($A_3$) 3D representation of the spatial variation of the $x$-component of the field between the tips of the iron bars, measured at the expected height of the rod. (B) Cross section of the sample cell made of various thickness coverslips glued together. The rod water solution was flowed into the cells and left for about 15–30′ to sediment on the hang-over made by the inner coverslip. The sample was then set upside-down on the microscope stage. ($C_1$) Bright field image of a rod stuck at one extremity (left side) on the inner coverslip. Scale bar = 5 μm. ($C_2$) Reflection image of the same rod. ($C_3$) Shows three typical grey intensity profiles along a rod cross-section (such as indicated by the yellow line on $C_2$) fitted by our theoretical model to measure the radius (yielding $r$ = 148 ± 8, 386 ± 7 and 476 ± 6 nm respectively for the red, blue and green curves). The red curve is taken from the rod shown on $C_2$.

properties (each particle has a single Weiss magnetization domain) and their size dispersity accounts for the divergence between the Langevin law and the magnetization curve of the particle ferrofluid suspension.[5] This result was confirmed by our own magnetization curves (ESI,† Fig. S2) of a ferrofluid suspension of the negatively charged (citrated) nanoparticles (volume fraction $\phi^v$ = 3.9%) obtained by VSM. This curve also yielded the log-normal distribution of the particle diameters (10–16 nm range, mean = 13 nm).[16] Following an already published protocol,[11] the rods were then prepared by dialysis of a solution of the nanoparticles mixed with positively charged polymers (poly(diallyldimethylammonium chloride)) while being exposed to a $\sim$250 mT magnetic field. We used a microscopic setup equipped with magnetic tweezers designed to induce a uniform magnetic field on the sample (Fig. 1). We carefully calibrated the field, and checked that the influence of the gradient was negligible.[11] To prepare the samples, we flowed a 100× diluted rod solution into an observation chamber, so that some of the rods were found in a cantilevered configuration, *i.e.* with a small part of the rod stuck on an inner coverslip while the longest part remained far from any solid surface (Fig. 1B). After performing the measurements, we checked that the clamped boundary condition was fulfilled by controlling the anchorage resisted to a large deformation induced by a magnet brought at the vicinity of the sample. The rods were observed using a DMIRB inverted Leica microscope equipped with an apo plan 100× NA 1.3 objective and a Photometrics fx-Coolsnap camera (pixel size (4.65 μm)$^2$) either by bright field or by reflection microscopy (Fig. 1C). Home made software programs were written to automatically pilot the magnetic tweezers and the camera, track noisy motion of the sample and digitize the rod shape with a resolution of 2–20 nm.[11]

Before performing the complete set of measurements on individual rods, we checked the validity of each of them. To characterize the rod geometry, the measurement of $L \sim$ 30–80 μm was straightforward on the images taken using the microscope, but the measurement of $r \sim$ 300 nm was more challenging because of the optical diffraction limit. We thus developed a theoretical model to compute the rod reflection intensity profile:

$$I_r(x) = I_0 + I_1 \int_{-r}^{r} \exp\left[-\frac{(s-x-x_0)^2}{2\sigma_{xy}{}^2}\right] 2r\sqrt{1-\left(\frac{s}{r}\right)^2}\,\mathrm{d}s,$$ where $I_0$ is the background intensity, $I_1$ is an effective intensity, $\sigma_{xy}$ is a function of the wavelength and the objective numerical aperture,

 

and $x$ is the abscissa along the rod cross section (ESI,† note 1). The value of $r$ was then obtained from the fit of this function to the experimental intensity measured at each rod cross-section (Fig. 1C). We checked our model by comparing its result to the value of $r$ measured by AFM on the same sample rods (ESI,† note 1 and Fig. S3). We found that the uncertainty of this optical measurement was of $\sim$30 nm, which is also the typical standard deviation of $r$ along the rod.

The mechanical characterization of the rod was previously fully described[11] and consisted of acquiring $\sim$900 images of the rod to analyze its thermal fluctuations, from which the rod persistence length $L_p$, its bending modulus $C = L_p/k_BT$ ($k_BT$ is the thermal energy) and its Young modulus $Y = \frac{4C}{\pi r^4}$ were deduced.[13]

The magnetic susceptibility $\chi$ of the rod material (defined as $\chi = \frac{M}{H}$, where $M$ is the magnetization and $H$ the field inside the material) was deduced from magnetoelastic experiments in which we analyzed the deflection of the rod deformed by a uniform field. During such magnetic deformation, the magnetic torque per unit volume $\Gamma_m = ||\vec{M} \wedge \vec{B}_0||$ ($\vec{B}_0$ is the uniform induction field) acting on the rod is counter-balanced by the elastic restoring torque $\frac{C}{R}$, $R$ being the local radius of curvature.[13] As shown in the ESI,† note 2, $\Gamma_m = \Delta\chi \sin(2\alpha)\frac{\pi r^2 B_0^2}{2\mu_0}$, where $\mu_0$ is the vacuum permeability, $\alpha$ is the angle of $\vec{B}_0$ with respect to the rod main axis and $\Delta\chi$ a function of $\chi$ and of the local components of the field $\vec{H}$ in the rod. Thus, the measurement of the rod deflection $\delta$ (Fig. 2A) may yield either one of the parameter $C$ or $\chi$ when the other one is known. However, a difficulty arises from the fact that $\chi$ depends on $H$. This can be directly observed on the magnetization curve of the nanoparticles before they were embedded in the rods (ESI,† Fig. S2) which shows deviation from linearity even at a very low field ($\chi^v$ varies by more than a factor of 2 between 2 and 10 mT). Consistently, previously detailed[11] viscous drag *versus* magnetic torque (VD/MT) experiments (in which the magnetically driven rotational kinetics of the free rods in solution is analyzed) also showed that the rod material susceptibility $\chi$ depends on $H$ and is proportional to $\chi^v$, the constant ratio $\chi/\chi^v$ being simply the ratio of the magnetic nanoparticle volume fraction within the rod and in the initial ferrofluid $\phi/\phi^v$.‡

Thus, to analyze the magnetoelastic experiments, we modified a theoretical model[12] to study the magnetoelastic deformation of low susceptibility rods. Although this model is only detailed here (ESI,† note 2), we showed that it matched accurately the shape of the deformed rods.[11] This model takes into account the dependence of $\chi$ on $H$, a variability which is often neglected.[2,7,9,19] Here, we also report experiments aimed at controlling that this model yields a constant measurement of $\phi$ independently of the field incidence and strength (Fig. 2). Fig. 2B shows experiments on a 33.1 μm long rod oriented at various incidence angles $\theta_0$ from 0 to 60° in a constant applied field. The deflection $\delta(\theta_0)$ (Fig. 2A) varies accordingly to our theoretical model: when $\theta_0$ varies, so does the internal field $H$ (ESI,† Fig. S4) and we found that despite this variation, the measured ratio $\frac{\chi(H)}{\chi^v(H)}$ remained constant. Consequently the comparison also yielded a fairly constant value for $\phi$ (within ±2%). This experiment and the theoretical curves shown in Fig. 2A also suggested that the best values at which these deflection measurements should be performed were $\theta_0 \sim$ 30–50: at these angles, the deflection $\delta$ reaches a maximum plateau when $B_0$ is below the magnetoelastic buckling field.[12]

Next, at a constant incidence $\theta_0 = 35 \pm 0.1$, we studied the effect of the field intensity on the rod deflection (Fig. 2C). We monitored 130 deformations of a 46.4 μm long rod subjected to an incrementally increased intensity of the external induction field from 0 to 7 mT. The fields were successively turned on during 500 ms (a sufficient time to reach the equilibrium configuration) and off for the same amount of time to monitor the rod returning to its undeformed state. Excepted the thermal fluctuations, the deformations were reproducible. They did not increase incrementally, an effect which could have occurred in the case of remanent magnetization, thus confirming the superparamagnetism of the rod. During this experiment, the rod deflected by a maximum of 1.6 μm (corresponding to a deviation of 2°), and the induced longitudinal field $\mu_0 H_{0\parallel}$ ranged from 0 to 4 mT. The analysis of the deflection according to the theoretical model showed that $\chi(H_{0\parallel})$ varied by more than a factor of two, but remained proportional to $\chi^v(H_{0\parallel})$. The values found for $\chi$ below 2 mT (for which no VSM data are available) also appeared consistent with the expected shape of the magnetic susceptibility curve. The deduced measurements of $\phi$ were found to vary by less than 10% and yielded a mean value of $\langle\phi\rangle = 15\% \pm 0.8$.§ In contrast, if $\chi$ is assumed constant, $\phi$ varies by a factor of two when deduced from these measurements.

We then proceeded to the full characterization of ten individual rods. All came from the same synthesis batch. Once $L$, $r$ and $C$ were determined as described above, the measurement of $\chi$ consisted in subjecting the rod to $\sim$1 s long pulses of magnetic field applied at a 35° incidence. The field intensity was varied from $\sim$2 to $\sim$8 mT to check the constancy of $\phi$ for a given rod. At each field intensity, the measurements were repeated 5 times to average out the errors mostly due to the thermal fluctuations ($\sim$1/10 of the magnetic deflections) (ESI,† Fig. S5A and Movie 1). The deflections always remained small ($\delta \sim 1$ μm, $\theta_L \lesssim 1$), which also ensured that the system was probed in the linear elastic regime: for larger deformations, we observed a plastic behavior (ESI,† Fig. S5B). To monitor small deformations, we took advantage of our super-resolutive image analysis algorithm[11] to measure the rod centerline from the microscopy images with a precision of a few tens of nanometers (ESI,† Movie 1).

Table 1 shows the results for 10 rods selected over nearly 100 studied samples. Reasons for rejections were insufficiently straight or badly anchored rods, or uncontrolled vibrations of the sample (noise) which prevented the detection of the thermal fluctuations. The selected rods were homogeneous in length because we chose the longest to allow a fine detection of

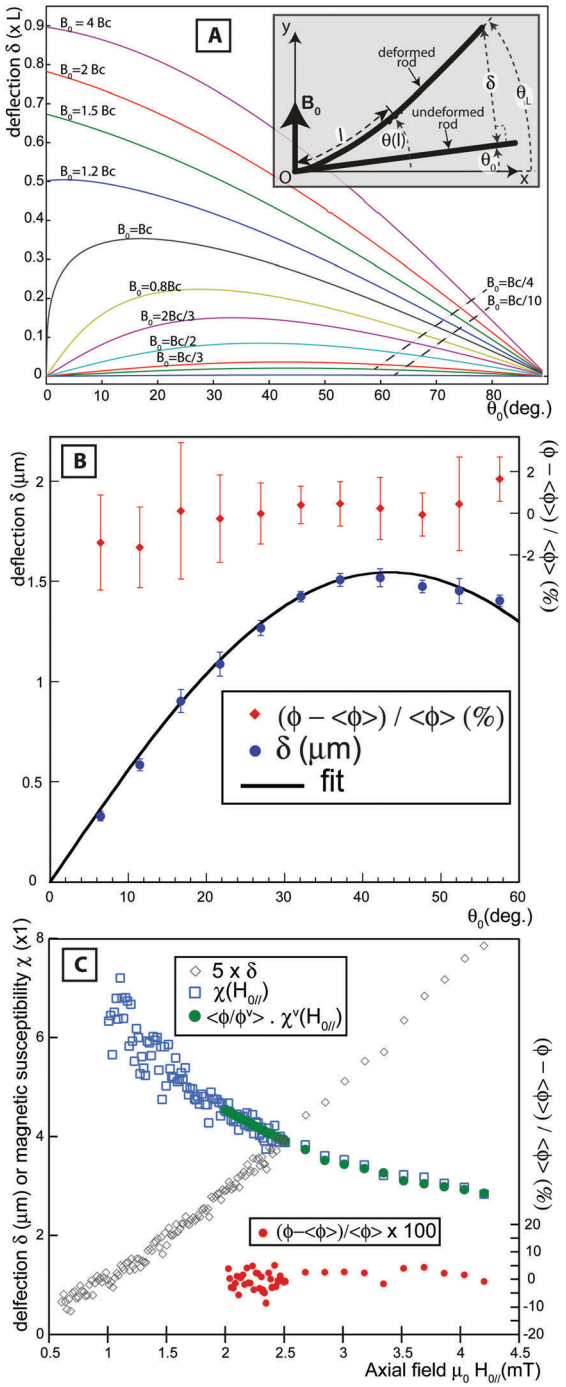


Fig. 2 Magnetoelastic experiments. (A) Inset: Notations used to describe the magnetoelastic experiments, indicating in particular the deflection $\delta$ of the rod tip. Main curve: theoretical computations of $\delta$ using the "axial model" for a cantilevered rod of length $L = 1$ as a function of the incidence angle $\theta_0$ of the field. Each curve corresponds to a magnetic induction intensity $B_0$ given relatively to the magnetoelastic buckling critical field $B_c$. For all curves such that $B_0 \leq B_c$ the deflection is close to a maximum when $\theta_0 \sim 35$–$50°$. (B) Experimental data with a $33.1 \pm 0.05$ μm long rod ($C = 1.6 \times 10^{-20}$ Jm) probed at 11 incidence angles with $B_0 = 4.8 \pm 0.15$ mT. The deflection $\delta$ (blue dots) is in excellent agreement with the theoretical curve of the axial model (solid black line) which corresponds to the "$B_0 = B_c/4$" curve of (A). The error bars indicate the dispersion of the 5 measures taken at each angle. Red diamonds (scale on the right $y$-axis) are $\frac{\phi - \langle\phi\rangle}{\langle\phi\rangle}$: the variation of the volume fraction $\phi$ (relatively to the mean of all values $\langle\phi\rangle$), computed from $\delta$ (see the text and ESI,† note 2). The variation remain below ±2%, indicating the independence of the measurement with $\theta_0$. (C) Analysis of the deflection of a cantilevered microrod ($r = 0.34 \pm 0.04$ μm, $L = 46.37 \pm 0.05$ μm, $C = 300 \pm 80 \times 10^{-21}$ Jm) bent by an incrementally increased intensity of the magnetic induction field applied at $\theta_0 = 35$. The field $B_0$ varies from 0 to 4 mT by 0.027 mT steps and by 0.27 mT steps from 4 to 7 mT to reduce heating of the induction coils. The following quantities are plotted as a function of $B_{0\parallel} = \mu_0 H_{0\parallel}$ (the projection of the field along the direction of the rod tip): 1 – (along the left-axis) $5 \times \delta$ (black diamonds) from which are computed $\chi(H_{0\parallel})$ (blue squares), and $\langle\phi/\phi^v\rangle \times \chi^v(H_{0\parallel})$ (green dots) the magnetic susceptibility of the ferrofluid nanoparticles extrapolated at the mean volume fraction $\langle\phi\rangle$ of the particles in the the rod (VSM data are available only above 2 mT), and 2-(along the right-axis) $\frac{\phi - \langle\phi\rangle}{\langle\phi\rangle}$ (filled red circles) as in (B). The transverse field $\mu_0 H_\perp$ (not plotted) varies from 0.11 to 1.5 mT and is taken into account for the computations of $\phi$.

 

Table 1 Results for 10 rods

| No. | $L$ (μm) | $r$ (μm) | $C$ ($\times 10^{-21}$ Jm) | $Y$ (MPa) | $\chi$@4mT ($\times 1$) | $\phi$ (%) | Part./rod ($\times 1000$) | Part./Cr.-Sec. ($\times 1$) |
|---|---|---|---|---|---|---|---|---|
| 1 | 34.36 ± 0.05 | 0.316 ± 0.027 | 21.5 ± 4 | 2.7 ± 1.5 | 2.4 ± 0.9 | 9.2 ± 3.4 | 108 ± 59 | 82 ± 45 |
| 2 | 26.83 ± 0.05 | 0.302 ± 0.001 | 38.1 ± 16 | 5.8 ± 3.1 | 4.1 ± 1.7 | 15.8 ± 6.6 | 132 ± 66 | 128 ± 64 |
| 3 | 44.92 ± 0.05 | 0.366 ± 0.024 | 398 ± 74 | 28.3 ± 12.6 | 3.0 ± 1.0 | 11.4 ± 4.0 | 234 ± 115 | 135 ± 67 |
| 4 | 35.94 ± 0.05 | 0.372 ± 0.027 | 76.7 ± 14.3 | 5.1 ± 2.4 | 2.00 ± 0.7 | 7.7 ± 2.7 | 130 ± 67 | 94 ± 49 |
| 5 | 54.17 ± 0.05 | 0.410 ± 0.080 | 42.8 ± 8.0 | 1.9 ± 1.9 | 2.5 ± 1.4 | 9.75 ± 5.2 | 303 ± 281 | 145 ± 135 |
| 6 | 42.41 ± 0.05 | 0.320 ± 0.013 | 448 ± 84 | 54 ± 19 | 7.4 ± 2.4 | 28.5 ± 9.1 | 422 ± 174 | 259 ± 107 |
| 7 | 55.70 ± 0.05 | 0.330 ± 0.040 | 536 ± 100 | 58 ± 39 | 5.3 ± 2.4 | 20.3 ± 9.4 | 420 ± 299 | 196 ± 140 |
| 8 | 25.52 ± 0.05 | 0.314 ± 0.024 | 154.0 ± 29 | 20 ± 10 | 3.4 ± 1.3 | 13.4 ± 5.0 | 115 ± 62 | 117 ± 64 |
| 9 | 42.31 ± 0.05 | 0.301 ± 0.014 | 30.3 ± 5.7 | 4.7 ± 1.8 | 2.6 ± 0.9 | 10.0 ± 3.6 | 131 ± 60 | 81 ± 37 |
| 10 | 36.41 ± 0.05 | 0.331 ± 0.037 | 158 ± 30 | 16.8 ± 11 | 5.5 ± 2.3 | 21.0 ± 8.7 | 285 ± 185 | 204 ± 132 |
| Mean | 39.86 | 0.336 | 190.4 | 19.8 | 3.8 | 14.7 | 228 | 144 |
| SD | 10.15 | 0.035 | 196 | 21 | 1.7 | 6.7 | 124 | 59 |

Measured parameters of 10 microrods from the same batch. The standard deviation for $L$ indicates the uncertainty of the measurement (estimated as a pixel size at each rod end). For $r$, the value is the mean ± SD of the variation of the measurements along the rod (the precision of a single measurement being 30 nm). For $C$, $\chi$ and $\phi$ the value is provided with the experimental uncertainty of the measurements. From these values, we estimate the total number of particles in each rod and per cross-section. The last two lines are the mean and SD of each parameter for the 10 analyzed rods.

the thermal fluctuations. This selection might also explain the small dispersion in thickness as $r$ varies only from 0.3 to 0.4 μm. By contrast the flexural rigidity was extremely variable, ranging from 21.5 to 536 $\times$ $10^{-21}$ Jm, corresponding to a persistence length from 5 to 130 m and a Young modulus of 2 to 60 MPa. The measured susceptibility (for $B_0$ = 4 mT) was found to vary by a factor of 3 ($\langle\chi\rangle$ = 3.8 ± 1.7) as the volume fraction ($\langle\phi\rangle$ = 14.7 ± 6.7) and the mean particle number per rod cross-section: 144 ± 59.¶

In these measurements, the final precision of only 25–50% on $\chi$ and $\phi$ mostly arises from the uncertainty on $C$, due to the difficulty to detect the small fluctuations of the rods (~10–100 nm[11]). However, this precision was sufficient to display the large disparity of the rod characteristics, unreported by the previous study on the stiffness of such rods[2] which contained a single measurement. This surprisingly high dispersion is corroborated by several observations: (i) several previous papers concerning these types of rods also reported a large distribution of their properties such as their log-normal distribution of lengths[9] or their susceptibility[7] which was plotted on a logarithmic scale; (ii) the VD/MT experiments performed on ten other rods gave a similar range of values for $\chi$ = 4.6 ± 1.2 (for $B_0$ = 4 mT), which consistently yielded a similar result for $\langle\phi\rangle$ = 17.8 ± 4.5%;[11] (iii) the alternative analysis of the magnetoelastic experiments (in which $\chi$ is set from the VD/MT experiments and $C$ is looked for) confirmed the values of $C$ determined using the thermal fluctuation method,[11] and in particular (iv), the fact that despite their large variation and the complete independence of their measurements, the combination of values found for $C$ and $\chi$ yielded consistent results for $\phi$ = 14.7 ± 6.7% which fall into a narrow acceptable range of values: from electron micrographs,[19] it has to be above 10% but also below 50%, the fraction of randomly close-packed spheres. By comparison, a small angle neutron scattering study on isotropic aggregates made of different kinds of polymers and smaller nanoparticles yielded a mean value for $\phi$ = 38%.[8] In the present study, the large dispersion of values highlights the advantage of fully characterizing each rod individually: if we had only known a mean value for $C$ from a distribution of rods, the magnetoelastic experiments would have yielded results for $\chi$ ranging from 0.6 to 13 and inconsistent values of $\phi$ from 2.3 to 60%!

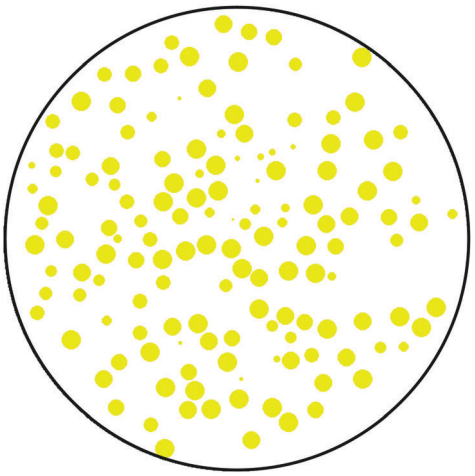

Fig. 3 Simulation of 144 nanoparticles (ø = 13 nm) (mean value found for the 10 analyzed rods detailed Table 1) randomly distributed in a cross-section of a rod of radius $r$ = 300 nm.

This study shows that the number of nanoparticles per rod cross-section is relatively small (Fig. 3), thus indicating that rods with a higher concentration of particles could be synthesized to obtain a greater magnetic susceptibility. This information on the microscopic structure also suggests that the rod stiffness is mostly dictated by the polymer matrix. A putative explanation of the rod stiffness variability is that fluctuations in numbers of particles from one rod to another yield even larger fluctuations of the concentration $c$ in polymer chains, which adsorb onto the particles. This must induce variable elastic properties according to the scaling law of a polymer mesh $Y \propto c^{2.2}$.[15] For future uses, a sorting or a more selective method to produce the rods more homogeneously needs to be developed. Meanwhile, individual rod characterization as described in this paper may be required for many applications. We also

believe that insights could be gained on numerous other types of magnetic microrods from the techniques we have introduced here.

## Acknowledgements

The authors thank M. Devaud for fruitful discussions and his patient proof-reading of the manuscript.

## References

‡ For non-interacting and uniformly magnetized nanoparticles such as used here, magnetization (and therefore susceptibility) is simply proportional to the volume of magnetic matter.[10]
§ The standard deviation of 0.8% only accounts for the variability of the measurements and not for the uncertainty of the other previously independently determined parameters (see Table 1).
¶ The uncertainty for these numbers is the standard deviation of the measurements on the 10 rods.

1 J. C. Bacri, R. Perzynski, D. Salin, V. Cabuil and R. Massart, Magnetic colloidal properties of ionic ferrofluids, *J. Magn. Magn. Mater.*, 1986, **62**(1), 36–46.
2 L. Chevry and J.-F. Berret, Sub-piconewton force detection using micron-size wire deflections, *RSC Adv.*, 2013, **3**(38), 17254.
3 R. Colin, L. Chevry, J.-F. Berret and B. Abou, Rotational microrheology of Maxwell fluids using micron-sized wires, *Soft Matter*, 2014, **10**(8), 1167–1173.
4 R. S. Devan, R. A. Patil, J. H. Lin and Y. R. Ma, One-dimensional metal-oxide nanostructures: Recent developments in synthesis, characterization, applications, *Adv. Funct. Mater.*, 2012, **22**(16), 3326–3370.
5 W. C. Elmore, The Magnetization of Ferromagnetic Colloids, *Phys. Rev.*, 1938, **54**(12), 1092–1095.
6 A. Fert and L. Piraux, Magnetic nanowires, *J. Magn. Magn. Mater.*, 1999, **200**, 338–358.
7 J. Fresnais, J. F. Berret, B. Frka-Petesic, O. Sandre and R. Perzynski, Electrostatic co-assembly of iron oxide nanoparticles and polymers: Towards the generation of highly persistent superparamagnetic nanorods, *Adv. Mater.*, 2008, **20**(20), 3877–3881.
8 J. Fresnais, J. F. Berret, L. Qi, J. P. Chapel, J. C. Castaing, O. Sandre, B. Frka-Petesic, R. Perzynski, J. Oberdisse and F. Cousin, Universal scattering behavior of coassembled nanoparticle-polymer clusters, *Phys. Rev. E: Stat., Nonlinear, Soft Matter Phys.*, 2008, **78**(4), 20–23.
9 B. Frka-Petesic, K. Erglis, J. F. Berret, A. Cebers, V. Dupuis, J. Fresnais, O. Sandre and R. Perzynski, Dynamics of paramagnetic nanostructured rods under rotating field, *J. Magn. Magn. Mater.*, 2011, **323**(10), 1309–1313.
10 F. Gazeau, E. Dubois, J. C. Bacri, F. Boue, A. Cebers and R. Perzynski, Anisotropy of the structure factor of magnetic fluids under a field probed by small-angle neutron scattering, *Phys. Rev. E: Stat., Nonlinear, Soft Matter Phys.*, 2002, **65**(3), 1–15.
11 F. Gerbal and Y. Wang, Optical detection of nanometric thermal fluctuations to measure the stiffness of rigid superparamagnetic microrods, *Proc. Natl. Acad. Sci. U. S. A.*, 2017, **114**(10), 2456–2461.
12 F. Gerbal, Y. Wang, F. Lyonnet, J. Bacri, T. Hocquet and M. Devaud, A refined theory of magnetoelastic buckling matches experiments with ferromagnetic and superparamagnetic rods, *Proc. Natl. Acad. Sci. U. S. A.*, 2015, **112**(23), 7135–7140.
13 L. D. Landau and E. M. Lifshitz, *Theory of Elasticity*, Pergamon press, Oxford, 2nd edn, 1970.
14 X. Liang, J. Liu, S. Li, Y. Mei and W. Yanqing, Magnetic and mechanical properties of micro/nano particles prepared by metallizing rod-shaped bacteria, *Mater. Lett.*, 2008, **62**(17–18), 2999–3002.
15 F. C. MacKintosh, J. Käs and P. A. Janmey, Elasticity of Semiflexible Biopolymer Networks, *Phys. Rev. Lett.*, 1995, **75**(24), 4425–4429.
16 O. Sandre, J. Browaeys, R. Perzynski, J.-C. Bacri, V. Cabuil and R. Rosensweig, Assembly of microscopic highly magnetic droplets: Magnetic alignment *versus* viscous drag, *Phys. Rev. E: Stat. Phys., Plasmas, Fluids, Relat. Interdiscip. Top.*, 1999, **59**(2), 1736–1746.
17 H. Singh, P. E. Laibinis and T. A. Hatton, Synthesis of flexible magnetic nanowires of permanently linked core–shell magnetic beads tethered to a glass surface patterned by microcontact printing, *Nano Lett.*, 2005, **5**(11), 2149–2154.
18 J. W. Tavacoli, P. Bauër, M. Fermigier, D. Bartolo, J. Heuvingh and O. du Roure, The fabrication and directed self-assembly of micron-sized superparamagnetic non-spherical particles, *Soft Matter*, 2013, **9**(38), 9103–9110.
19 M. Yan, J. Fresnais, S. Sekar, J. P. Chapel and J. F. Berret, Magnetic nanowires generated *via* the waterborne desalting transition pathway, *ACS Appl. Mater. Interfaces*, 2011, **3**(4), 1049–1054.
20 V. Zhukova, M. Ipatov and A. Zhukov, Thin magnetically soft wires for magnetic microsensors, *Sensors*, 2009, **9**(11), 9216–9240.

 